

# BEV<sup>2</sup>PR: BEV-Enhanced Visual Place Recognition with Structural Cues

Fudong Ge<sup>1,2\*</sup>, Yiwei Zhang<sup>1,2\*</sup>, Shuhan Shen<sup>1,2</sup>, Yue Wang<sup>4</sup>, Weiming Hu<sup>1,2,3</sup>, Jin Gao<sup>1,2†</sup>

**Abstract**—In this paper, we propose a new image-based visual place recognition (VPR) framework by exploiting the structural cues in bird’s-eye view (BEV) from a single monocular camera. The motivation arises from two key observations about VPR: 1) For the methods based on both camera and LiDAR sensors, the integration of LiDAR in robotic systems has led to increased expenses, while the alignment of data between different sensors is also a major challenge. 2) Other image/camera-based methods, involving integrating RGB images and their derived variants (e.g., pseudo depth images, pseudo 3D point clouds), exhibit several limitations, such as the failure to effectively exploit the explicit spatial relationships between different objects. To tackle the above issues, we design a new BEV-enhanced VPR framework, namely BEV<sup>2</sup>PR, which can generate a composite descriptor with both visual cues and spatial awareness solely based on a single camera. For the visual cues, any popular aggregation module for RGB global features can be integrated into our framework. The key points lie in: 1) We use BEV segmentation features as an explicit source of structural knowledge in constructing global features. 2) The lower layers of the pre-trained backbone from BEV map generation are shared for visual and structural streams in VPR, facilitating the learning of fine-grained local features in the visual stream. 3) The complementary visual features and structural features can jointly enhance VPR performance. Our BEV<sup>2</sup>PR framework enables consistent performance improvements over several popular camera-based VPR aggregation modules when integrating them. The experiments on our collected VPR-NuScenes dataset demonstrate an absolute gain of 2.47% on Recall@1 for the strong Conv-AP baseline to achieve the best performance in our setting, and notably, a 18.06% gain on the hard set. The code and VPR-NuScenes dataset will be available at <https://github.com/FudongGe/BEV2PR>.

## I. INTRODUCTION

Visual Place Recognition (VPR) plays a crucial role in robotics and autonomous driving, typically framed as an image retrieval task [1], [2], [3]. The primary objective of a VPR system is to ascertain the spatial position of a provided query image, involving the initial extraction of its visual information into a compact representation, and a subsequent comparison with a reference database with known geolocations. These image-based methods are susceptible to challenges such as varying illumination and weather, attributed to the intrinsic characteristics of camera sensors [4]. Therefore, a question arises naturally: *How to learn a robust representation for VPR based solely on cameras?*

\* Equal contribution

† Corresponding author (jin.gao@nlpr.ia.ac.cn)

<sup>1</sup> State Key Laboratory of Multimodal Artificial Intelligence Systems (MAIS), CASIA

<sup>2</sup> School of Artificial Intelligence, University of Chinese Academy of Sciences

<sup>3</sup> School of Information Science and Technology, ShanghaiTech University

<sup>4</sup> State Key Laboratory of Industrial Control Technology and Institute of Cyber-Systems and Control, Zhejiang University

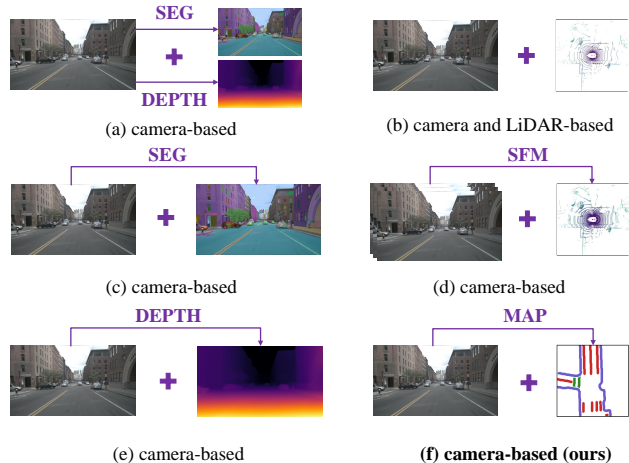


Fig. 1. Schematic diagram of methods based on both appearance and structure using camera and/or LiDAR sensors: a) methods using RGB, segmentation and depth images, b) methods using RGB images from camera and 3D point clouds from LiDAR, c) methods using RGB and segmentation images, d) methods using RGB images and 3D point clouds reconstructed from multiple RGB images, e) methods using RGB and depth images, f) (ours) using RGB images and BEV generated from RGB images.

When locating, the human brain typically relies on the sights observed by eyes, including the colors of scenes, the textures of objects’ surfaces, and the spatial structure perception learned through years of experience. Therefore, it’s possible to construct a robust representation with both appearance and structural properties solely based on the camera. After reviewing the development progress of VPR technology, we find that the research based on both appearance and structure is a hotter field compared to studies solely based on appearance or structure [5], [6], [7]. As depicted in Fig. 1, existing methods based on both appearance and structure can be divided into approaches using both camera and LiDAR sensors [5], [6], [7], *i.e.*, (b), and camera-based approaches [8], [9], [10], *i.e.*, (a), (c), (d) and (e). Furthermore, the structural information sources of camera-based methods include reconstructed 3D point clouds, 2D segmentation images, 2D depth images, thus (c) *v.s.* (d) *v.s.* (e) is also a focus worth analyzing.

Upon examining the current methods, it is noted that each possesses its own advantages and disadvantages. The methods based on both camera and LiDAR in Fig. 1(b), which utilize the complementarity of multimodal raw information, face an issue involving higher procurement costs and maintenance expenses, as well as the calibration and alignment of different modal data [5], [6], [7]. Vehicles not equipped with LiDAR cannot deploy such algorithms. The SfM (Structure-from-Motion)-based methods with pseudo-

3D point clouds reconstructed from RGB images, *i.e.*, Fig. 1(d), reduces the costs of traditional approaches. However, this reconstruction process is relatively complex, and the data required for inference are more challenging to handle than conventional pixel images [9]. Moreover, this method highly depends on the quality and coverage of the images. If the images are of poor quality (for example, blurred due to rain), or if there is insufficient coverage between different images, it may lead to low-quality reconstructed point clouds, thereby impacting the accuracy. Beneficial from current segmentation models [11], SEG-based methods in Fig. 1(c) use segmentation images to enhance structural knowledge of global features. However, segmentation images are still in the x-y 2D plane without the implicit structure - depth, resulting in the loss of key information. Fig. 1(e) provides depth information, while depth images contain harmful noise from dynamic objects, and lack explicit spatial relationships between different objects. The limitations of the current methods raise a question: *Could we integrate explicit depth and spatial relationships as well as RGB information into global features using images as input during inference?*

To tackle this issue, we propose our solution - **RGB and BEV fusion**, inspired by the widespread application of BEV representations in 3D perception tasks, where BEV exhibits outstanding performance in clearly depicting the relative positions and shapes of objects. The challenge lies in *how to integrate BEV features into global features and how to leverage the knowledge in structural stream to enhance visual stream*. Therefore, we propose a new architecture, **BEV<sup>2</sup>PR**, which is designed to simultaneously construct semantic map to model spatial relationships in the **BEV** frame, and generate a composite descriptor with both visual cues and spatial awareness for **VPR**. Specifically, we first pre-train a BEV generation model to extract BEV features as a more explicit source of structural knowledge. And we copy the modules of the BEV model as part of the structural stream and freeze them to introduce BEV features into VPR, then crop its backbone into two parts, with the former serving as the bottom backbone shared with the visual stream and the latter copied as the sub-backbone of visual stream and then unfrozen. After that, any popular aggregation module for RGB global features is inserted into the visual stream, followed by a fusion operation. In particular, our framework only uses images as input, without involving other sensors or complex training processes, making it generalized for a wide range of autonomous vehicles.

Our main contributions can be highlighted as follows: 1) **Data Module**: We introduce VPR-NuScenes to distinguish between simple and challenging scenes to understand the respective strengths of visual and structural representations. 2) **Architecture**: We propose BEV<sup>2</sup>PR to simultaneously construct semantic map to model spatial relationships in the BEV frame, and generate a composite descriptor with both visual cues and spatial awareness for VPR. 3) **Experimental Results**: We conduct extensive experiments to evaluate the improvement effect of our framework on different appearance-based methods, particularly in scenes

characterized by significant appearance variations.

## II. RELATED WORK

The related work in this paper broadly involves appearance-based place recognition as well as place recognition based on both appearance and structure. The former focus on studying the semantic and texture information of RGB images, while the latter introduces structural information on the basis of the former.

### A. Place Recognition based on Appearance

The appearance-based place recognition concentrates on constructing better image representations including global or local descriptors for retrieval, where global descriptors can be generated through direct extraction or by aggregating local descriptors [10]. As a representative of aggregation technology, NetVLAD [12] is a trainable variant of VLAD, softly allocating local features to a set of learned clusters. Based on it, many variants have been inspired, such as SPE-NetVLAD [13] and Gated NetVLAD [14].

Several methods emphasize identifying key regions within feature maps. One notable technique, GeM [15], represents a learnable variant of global pooling, expanding upon which, Berton *et al.* introduce CosPlace [16] that combines GeM with a linear layer, exhibiting strong performance. TransVPR [17] by Wang *et al.* integrates CNN with Transformer by multi-head self-attention mechanism to infuse attention within output tokens from Transformer encoder. In [18], Alibey *et al.* focus on processing the high-level features and propose Conv-AP, which implements channel-wise pooling on the features followed by spatial-wise adaptive pooling, achieving state-of-the-art results on multiple benchmarks.

### B. Place Recognition based on both Appearance and Structure

**Place Recognition Relying on LiDAR**. Considering the robustness of structural features in some environments, scholars have attempted to introduce the technology of fusing lidar and cameras into place recognition. PIC-Net [19] by Lu *et al.* employs global channel attention to enhance the interaction between image and point cloud features, along with a spatial attention-based VLAD to select the discriminative points and pixels. Zhou *et al.* develop LCPR [7], a multi-scale network leveraging self-attention mechanism to correlate panoramic features across different modalities. OneShot [20] by Ratz *et al.* projects the segments from point clouds onto images to facilitate feature extraction through 2D and 3D CNN. CORAL [21] by Pan *et al.* first builds an elevation image from lidar scans, and then augments it with projected visual features to generate a fusion descriptor in the BEV frame.

**Place Recognition Independent of LiDAR**. Another path relies solely on cameras. Oertel *et al.* [9] use structural features extracted from image sequences through vision-based SfM to augment VPR. Shen *et al.* [10] try to leverage segmentation images obtained from a pre-trained segmentation model to augment the structural comprehension embedded within global representations, achieving state-of-the-art

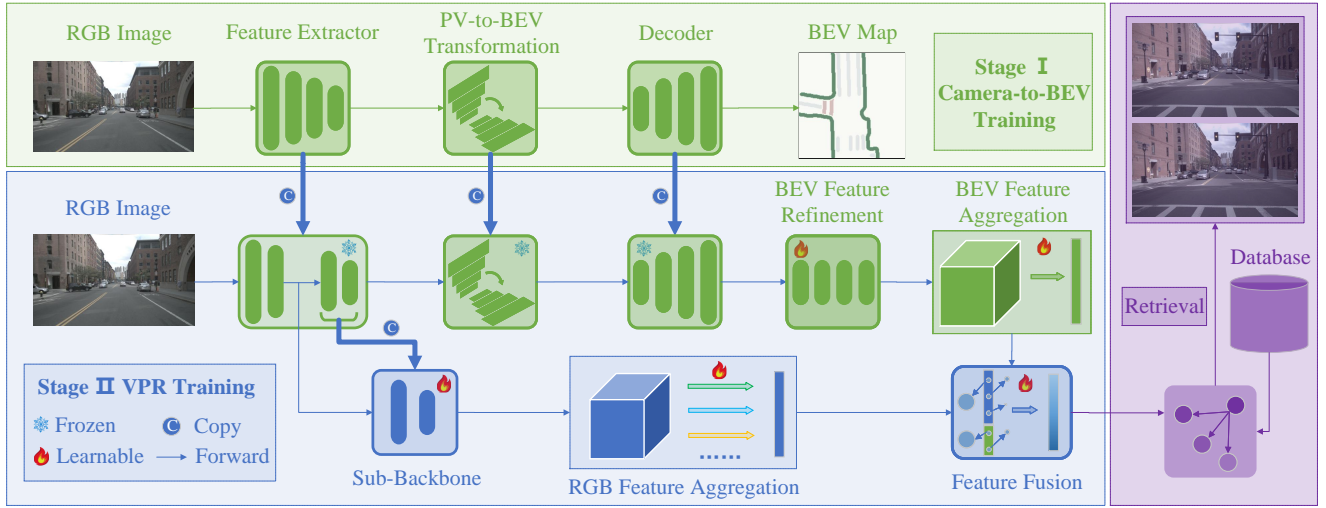


Fig. 2. Overview of our proposed pipeline. (1) In Stage I, we pre-train a BEV generation model using a front-view image to extract BEV features as a more explicit source of structural knowledge in the global feature. (2) In Stage II, we first copy the modules of the BEV model as part of the structural stream and freeze them to introduce BEV features into VPR, then crop its backbone into two parts, with the former serving as the bottom backbone shared with the visual stream and the latter copied as the sub-backbone of visual stream and then unfrozen. After that, any aggregation module for RGB global features is inserted into the visual stream and a relatively simple GeM module is used in the structural stream, followed by a feature fusion operation. (3) Finally, the nearest neighbor search is used to retrieval the Top-K images.

performance. Based on knowledge transfer and adversarial learning, Qin *et al.* [22] propose a structure-aware feature disentanglement network, called SFDNet, where probabilistic knowledge transfer is employed to transfer knowledge obtained from the Canny edge detector to the structure encoder. DASGIL [8] by Hu *et al.* uses multi-task architecture with a single shared encoder to create global representation.

Nevertheless, these previous works fail to simultaneously meet the requirements of low cost as well as explicit spatial relationships within global features. In this paper, we for the first time try to enhance VPR through a late-fusion approach of RGB features and BEV structural features.

### III. METHODOLOGY

Considering that BEV representation contains enriched and explicit structural knowledge, we attempt to leverage BEV features to infuse structural information into global retrieval. The core concept behind BEV<sup>2</sup>PR focuses on the static features in BEV images and the explicit spatial relationships between different objects, as well as the single-input but dual-modal processing method. BEV<sup>2</sup>PR involves two training stages: Camera-to-BEV training and VPR training, which is shown how to work in Fig. 2.

#### A. Overview

Given an input RGB image, a BEV generation model is pre-trained in the first training stage, by which BEV features can be obtained to assist in VPR. In the second training stage, the BEV model is frozen and its backbone is cropped into two sequential parts. Finally, we insert any global feature aggregation into visual stream, followed by a fusion operation to obtain a composite descriptor.

#### B. BEV Map Generation

**Semantic Class Selection.** In various BEV images, there are different numbers of semantic instances, making the selection of appropriate types and quantities significant. A BEV map is represented by a  $C \times H \times W$  tensor, where  $C$  represents the number of semantic classes, and  $H \times W$  corresponds to the area in front of the ego vehicle. Within this tensor, regions belonging to the  $c^{th}$  class are marked with positive values in the corresponding  $c^{th}$  channel, while all other channels are set to zero. And, in the context of VPR, we improve model convergence and accuracy by only using static classes as the target to train the BEV generation model. This technique draws inspiration from the fact that each semantic class plays a different role in VPR, and further human brain’s attention mechanism, which concentrates on iconic static elements or important regions, such as roads and buildings, while ignoring dynamic ones similar to noise.

**Camera-to-BEV Model.** In this section, we establish a BEV generation model with only a front-view image as input. First, an image is embedded by a 2D CNN to get the feature map. And then, we transform the feature map from 2D to 3D using a similar method with [23], that is 1) predict grid-wise depth distribution with equal spacing on 2D features, 2) ‘lift’ the 2D features to voxel space based on depth, obtaining a pseudo point cloud features. Finally, a pooling operation similar to LiDAR-based methods is implemented to flatten 3D point cloud features into 2D BEV features.

#### C. Structural Knowledge Extraction

**Shared Bottom Backbone.** Due to the insensitivity of global features to small targets in the raw visual stream, we adopt a shared bottom backbone instead of the architecture of separately processing input images in visual and structural

streams. To specify, we crop the backbone of BEV generation model into two sequential parts, with the former serving as a bottom backbone shared with the visual stream, so as to prompt visual stream to learn fine-grained local features generated by the BEV semantic segmentation, after which, a specific sub-backbone for the visual stream is used to capture important features for VPR. The experimental results in Section IV confirm its effectiveness.

**Feature Refinement Module.** Considering that the BEV feature map operates at a higher semantic level compared to the RGB image and needs to be refined to denoise and adapt to VPR, we adopt a part of depth stream in MobileSal [24] as the feature refinement module in the structural stream. Specifically, there are totally five stages with the same strides, the last of which is modified to refine BEV features.

#### D. Feature Aggregation

As shown in Fig. 2, there are two feature aggregation modules in visual and structural streams, one of which in the structural stream is set to use GeM. In our work, we evaluate multiple methods to verify the improvement effects of BEV features on them. The feature map in visual or structural stream is denoted as  $\mathcal{X} \subseteq \mathcal{R}^{H \times W \times K}$ .

- SPoC [25]: This technique involves aggregating the features extracted from CNN through sum pooling, *i.e.*,

$$f^{(s)} = \frac{1}{|\mathcal{X}_k|} \sum_{x \in \mathcal{X}_k} x, \quad (1)$$

where  $k \in \{1, \dots, K\}$ .

- NetVLAD [12]: As a representative of aggregation technology, it's a trainable variant of VLAD, softly allocating local features to a set of learned clusters, defined as

$$f^{(n)} = [f_1^T, f_2^T, \dots, f_S^T], \quad (2)$$

where  $S$  represents the number of cluster centers, and

$$f_s = \sum_{i=1}^N \frac{e^{w_s^T x_i + b_s}}{\sum_{s'} e^{w_{s'}^T x_i + b_{s'}}} (x_i - c_s), \quad (3)$$

where  $w_s, b_s$  and  $c_s$  are sets of trainable parameters for each cluster,  $N = H \times W$  represents the total number of features.

- GeM [15]: This method implements a parametric generalized-mean mechanism, which can assign a shared parameter per feature map. Owing to the differentiable nature of the pooling operation, the parameters can be learned as part of the back-propagation. GeM is defined as

$$f_k^{(g)} = \left( \frac{1}{|\mathcal{X}_k|} \sum_{x \in \mathcal{X}_k} x^{p_k} \right)^{\frac{1}{p_k}}, \quad (4)$$

where  $k \in \{1, \dots, K\}$ ,  $p$  represents the learnable parameter.

- Conv-AP [18]: This is a fully convolutional feature aggregation technique, which performs channel-wise pooling on the feature maps followed by spatial-wise adaptive pooling, making the architecture convolutional and the output dimensionality configurable. Conv-AP is defined as

$$f^{(c)} = AAP_{s_1 \times s_2}(\text{Conv}_{1 \times 1}(\mathcal{X})), \quad (5)$$

where  $s_1 \times s_2$  represents the number of spatial sub-regions.

- EigenPlaces [26]: As a variant that builds on GeM aggregator, EigenPlaces utilizes a GeM pooling and a fully connected layer with output dimension 512. It's defined as

$$f^{(e)} = FC(\text{GeM}(\mathcal{X})). \quad (6)$$

- MixVPR [27]: This work focuses on an isotropic all-MLP architecture, and utilizes feature maps extracted from a pre-trained backbone as an aggregation of global descriptors to integrate the global interaction among elements within each feature map through a cascade of feature mixing. First,  $\mathcal{X}$  is considered as a set of 2D  $H \times W$  features, *i.e.*,  $\mathcal{X} = \{X^i\}$ ,  $i = \{1, \dots, K\}$ , followed by a flattening operation, resulting in flattened feature maps  $\mathcal{X} \subseteq \mathcal{R}^{D \times K}$ , where  $D = H \times W$ . Then, it's fed into  $N$  Feature Mixer blocks, *i.e.*,

$$\mathcal{Z} = FM_N(FM_{N-1}(\dots FM_1(\mathcal{X}))). \quad (7)$$

Finally, two fully connected layers are used to reduce its dimension depth-wise (channel-wise) then row-wise, *i.e.*,

$$\mathcal{Z}' = \mathcal{W}_d(\text{Transpose}(\mathcal{Z})), \quad (8)$$

$$f^{(m)} = \mathcal{W}_r(\text{Transpose}(\mathcal{Z}')), \quad (9)$$

where  $\mathcal{W}_d$  and  $\mathcal{W}_r$  are the weights of two layers.

#### E. Feature Fusion

Here, we use a weighted concatenation with two learnable scalar weights  $w_v$  and  $w_s$  rescaling each of the vectors, and the final descriptor is given by

$$f = \text{concat}(w_v f_v, w_s f_s), \quad (10)$$

where  $f_v$  and  $f_s$  represent the feature vectors of visual stream and structural stream respectively.

#### F. Network Training

We train our compound network in a two-stage manner instead of the extremely slow single-stage method. The loss function in the first stage fully refers to existing work [23], [28]. Then, following [12], we adopt the triplet margin loss to train the second-stage network. To specify, each training iteration involves a mini-batch  $(q, P_q, N_q)$  consisting of one anchor, multiple anchor's positive matches and negative matches. More details on the partitioning of positive and negative samples can be found in Section IV.A. We define  $f(\cdot)$  as the function mapping input to its descriptor, and the loss function of each descriptor is defined as

$$\mathcal{L}_k = \frac{1}{N_{\text{pos}} N_{\text{neg}}} \sum_{i=1}^{N_{\text{pos}}} \sum_{j=1}^{N_{\text{neg}}} \mathcal{L}_{ij}, \quad (11)$$

where  $k \in \{F, R, B\}$  represent the type of three descriptors,  $N_{\text{pos}}$  and  $N_{\text{neg}}$  represent the number of positive and negative samples in each mini-batch,  $\mathcal{L}_{ij}$  represent a tuple loss, *i.e.*,

$$\mathcal{L}_{ij} = \max(d(f(q), f(p_i)) - d(f(q), f(n_j)) + m, 0), \quad (12)$$

where  $d(\cdot)$  computes the Euclidean distance of two descriptors, margin  $m$  is a constant.

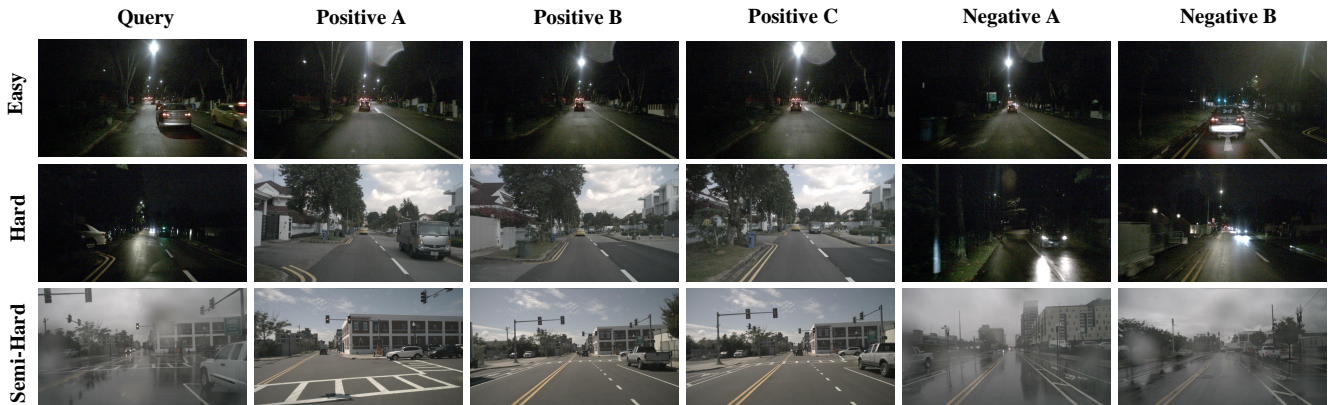


Fig. 3. Example of samples with different recall difficulties on our collected VPR-Nuscenes dataset.

TABLE I  
DEFINITION OF SAMPLE RECALL DIFFICULTY

Query \ Positive	Day	Night	Day&Rain	Night&Rain
Day	Easy	Hard	Semi-Hard	Hard
Night	Hard	Easy	Hard	Semi-Hard
Day&Rain	Semi-Hard	Hard	Easy	Hard
Night&Rain	Hard	Semi-Hard	Hard	Easy

TABLE II  
STATISTICS OF OUR DATA ORGANIZATION

	D	N	D&R	N&R	E	SH	H	Total	
								Scene	Sample
$N_{tr}$	14799	1239	3887	261	17335	1997	854	583	20186
$N_{te}$	5426	539	1176	124	5960	956	349	235	7265

$N_{tr}$  -  $N_{train}$ ,  $N_{te}$  -  $N_{test}$ ;

D - Day, N - Night, D&R - Day&Rain, N&R - Night&Rain;

E - Easy, SH - Semi-Hard, H - Hard.

Moreover, it has been reported in [5] that the network tends to overfit in image domain during training. Therefore, we use a multi-head loss function, denoted as

$$\mathcal{L}_{vpr} = \alpha \mathcal{L}_F + \beta \mathcal{L}_R + \gamma \mathcal{L}_B, \quad (13)$$

where  $\alpha, \beta, \gamma$  are constants determined by experiments.

## IV. EXPERIMENTS

### A. Dataset

Although there are multiple datasets available for VPR in challenging conditions, a deficiency is observed in annotated information for BEV semantic segmentation maps among them. Given our method’s dependence on BEV features for extracting structural information, evaluations are performed on the NuScenes [29], a public large-scale dataset for autonomous driving equipped with an entire suite of multi-modal sensors, including 6 cameras, 1 LiDAR, 5 radars, 1 IMU and 1 GPS. Among all the 1k scenes, each comprising a 20s-long sequence of consecutive frames, the trainval split includes 850 annotated scenes suitable for BEV generation, while the test split with 150 scenes has no annotations. Thus, only the annotated 850 scenes are eligible for our method.

**Partitioning of Positive and Negative Samples.** Given some characteristics that the spatial positions of consecutive frames are close and the camera angle changes are limited, while appearance such as illumination undergoes minimal variations, treating consecutive frames as positive samples proves excessively facile and lacks practical significance. Consequently, images within the same scene are not regarded as positive samples to one another. The selection of negative samples is straightforward: for each query sample, samples other than its positive samples and consecutive frames are defined as negative samples.

The exclusive reliance on GPS for distinguishing between positive and negative samples presents challenges. Images captured in close geographical location may fail to depict identical scenes when oriented differently, leading to pseudo positive samples. And variations in camera position while photographing the same site may introduce the possibility of pseudo negative samples. Due to the limitations in reflecting place position with camera coordinates, we employ image coordinates rather than camera coordinates for determining positive samples corresponding to a query sample.

In this work, the position of an image  $p_{img}$  is defined as 25m in front of the camera. In order to obtain more reasonable initial positive and negative samples, each image is represented by a binary tuple  $\langle p_{img}, v \rangle$ , where,  $v$  represents the directional vector of the camera-captured image, denoted as

$$v = p_{img} - p_{cam}, \quad (14)$$

where  $p_{cam}$  represents the position of the camera.

Then, we apply the Euclidean distance metric to calculate the distance between two images and those with a distance less than the threshold from other images are regarded as candidate positive samples, followed by calculating the angle between the direction vectors of query and positive to determine the final positive samples, *i.e.*,

$$\theta = \arccos\left(\frac{v_q \times v_{cp}}{\|v_q\| \|v_{cp}\|}\right), \quad (15)$$

where  $v_q$  and  $v_{cp}$  represent the direction vectors of the query image and the candidate positive images respectively.

Furthermore, in order to more clearly analyze the advantages and disadvantages of different modalities, we classify sample types based on the appearance differences between query and positive images, and define it as follows (refer to Table II for more details):

- **Hard Sample:** significant illumination difference. For instance, the query image is taken during daylight, while **all** positive images are captured at nighttime.
- **Semi-Hard Sample:** substantial contrast in image clarity due to precipitation. For example, the query is taken during the daytime, but **all** positive images are acquired in rain.
- **Easy Sample:** minimal appearance differences.

**Partition of Training and Test Sets.** Considering that NuScenes only involves four regions, each with data collected in relatively concentrated periods, we opt for a holistic partitioning approach for data across all areas. In VPR, the research on recalling from day to night, as well as from night to rain presents more challenges, but holds greater significance. Therefore, We aim to achieve a relatively uniform distribution of such data in both the training and testing sets. This data distribution design facilitates a more comprehensive evaluation of the model’s adaptability to complex environmental changes, enhancing the model’s generalization performance. *Note that there is no any instance and scene overlap between the training set and the test set.*

We first establish an undirected graph with scenes as nodes and similarity between scenes as edge weights, where the scene similarity is defined as the proportion of each query image in one scene that has a corresponding positive image appearing in another scene. Specifically, If all query images have positive images in the same scene, the scene similarity is set to 1. After processing all the scenes, there are 32 isolated scenes without connecting to any other scenes, making them unusable for VPR but usable for BEV generation. And the graph composed of other scenes involves 47 connected components. Finally, we leverage the official API of NuScenes dataset to acquire scene labels, such as "night" or "day", and based on which, the data is manually balanced, generating the partitioning results in Table I. *Further details are presented in <https://github.com/FudongGe/BEV2PR>.*

### B. Implementation Details

**Architecture.** We implement BEV<sup>2</sup>PR in PyTorch framework and only reproduce open-source models for a fair comparison, including SPoC [25], NetVLAD [12], GeM [15], Conv-AP [18], EigenPlaces [26], MixVPR [27]. For all techniques involving BEV generation and VPR, we use EfficientNet-B0 as the image backbone cropped at the last convolutional layer as recommended by their authors. Considering the information advantages of different scales, we adopt a method of upsampling the output of the 16<sup>th</sup> block and concatenating it with the output of the 11<sup>th</sup> block as final features. In addition, the sub-backbone in visual stream is cropped from the 12<sup>th</sup> block of EfficientNet-B0. The camera-to-BEV model outputs a 50m × 50m BEV map at a 25cm resolution with three classes, including lane boundary (Bound.), lane divider (Div.), and pedestrian crossing (P.C.),

*i.e.*,  $C = 3$ . Each input front-view image is resized from 1600 × 900 to 704 × 256 in all experiments for all models.

**Training.** During Stage I, we train the camera-to-BEV network using EfficientNet-B0 pre-trained on ImageNet for 40 epochs on four NVIDIA Tesla V100 GPUs. The Adam optimizer to update the weights of the network has a weight decay of  $1e^{-7}$  with a learning rate of  $1e^{-3}$ .

During Stage II, for maximum fairness in VPR, the final descriptor dimension of all methods is set to 640. We train the whole network using Adam optimizer having a weight decay of  $1e^{-3}$  with a learning rate of  $1e^{-5}$  for 40 epochs. For each mini-batch, the number of positive samples  $N_{pos} = 1$ , negative samples  $N_{neg} = 6$  and  $m = 0.5$  are set for the triplet loss. And the constants in the multi-head loss function are set to  $\alpha = 1$ ,  $\beta = 1$ ,  $\gamma = 1$ . In addition, we propose a newly online adaptive hard mining strategy to avoid model collapse caused by unstable gradients when the hard ratio is too high, as well as the neglect of samples rich in information when the hard ratio is too low. To specify, the hard ratio is dynamically adjusted based on loss changes.

**Evaluation.** The recall at Top-K (K = 1, 5, 10) is adopted as the evaluation metric, based on which, we evaluate our framework on the overall dataset as well as three subsets with different levels of recall difficulty, *i.e.*, R@K (overall), R<sup>E</sup>@K (easy), R<sup>H</sup>@K (hard), R<sup>SH</sup>@K (semi-hard).

### C. Evaluation for Visual Place Recognition

We apply six baseline models to our framework and evaluate the VPR performance based on monocular images. Table III shows the recall of methods on the VPR-NuScenes dataset. It can be seen that all methods incorporating structural streams have shown improvements in almost all metrics, with the absolute increments on R@1 across the overall dataset being 5.60%, 2.59%, 4.19%, 2.47%, 2.80%, 1.60%, and the ones on R@5 being 2.99%, 1.80%, 2.62%, 1.65%, 0.88%, 0.63%, respectively. We observe that the dual-stream models are relatively mediocre on the easy subset. Such results are due to the fact that models can achieve considerable performance using only appearance information under similar environments of illumination and weather, but also prove that datasets do not limit BEV<sup>2</sup>PR: on datasets with significant appearance differences, it can effectively improve performance (refer to next two paragraphs); on datasets with indistinct appearance differences, BEV<sup>2</sup>PR maintains RGB performance without hurting it.

**Illumination Change.** Compared to the easy set, the performance improvement on the hard set is more significant, with a maximum increase of 18.05% on R<sup>H</sup>@1. This can be attributed to the fact that in scenes with significant illumination changes, the semantic and texture information becomes completely ineffective and structural features in the BEV frame are relatively stable. As shown in the second row of Fig. 3, it’s difficult for human eyes to distinguish the complete scene, while just like in the nighttime scenes of autonomous driving in the real world, grounds are particularly clear compared to other areas, especially lane boundary and lane divider. Fig. 4 presents the RGB and BEV feature map

TABLE III  
EVALUATION OF VISUAL PLACE RECOGNITION PERFORMANCE.

Method	Year	Modality	BEV	R@1	R@5	R@10	R <sup>E</sup> @1	R <sup>E</sup> @5	R <sup>E</sup> @10	R <sup>H</sup> @1	R <sup>H</sup> @5	R <sup>H</sup> @10	R <sup>SH</sup> @1	R <sup>SH</sup> @5	R <sup>SH</sup> @10
SPoC [25]	2015	V	w/o	78.44	87.45	90.13	84.76	93.07	95.39	0.00	0.00	0.00	67.47	84.00	89.96
			w	84.04	90.44	92.27	89.70	95.14	96.39	10.60	12.89	16.62	75.52	89.44	94.14
Improvements	-	-	-	<b>+5.60</b>	<b>+2.99</b>	<b>+2.14</b>	<b>+4.95</b>	<b>+2.06</b>	<b>+1.01</b>	<b>+10.60</b>	<b>+12.89</b>	<b>+16.62</b>	<b>+8.05</b>	<b>+5.44</b>	<b>+4.18</b>
NetVLAD [12]	2016	V	w/o	88.26	92.49	93.73	94.09	97.41	98.43	2.01	4.58	6.88	83.68	94.04	96.23
			w	90.85	94.29	95.49	95.44	98.19	98.96	15.76	22.06	29.80	89.64	96.34	97.80
Improvements	-	-	-	<b>+2.59</b>	<b>+1.80</b>	<b>+1.76</b>	<b>+1.35</b>	<b>+0.78</b>	<b>+0.53</b>	<b>+13.75</b>	<b>+17.48</b>	<b>+22.92</b>	<b>+5.96</b>	<b>+2.30</b>	<b>+1.57</b>
GeM [15]	2018	V	w/o	80.14	88.01	90.17	86.22	93.38	95.25	0.00	1.72	2.87	71.23	85.77	90.06
			w	84.33	90.63	92.24	89.64	94.80	95.64	12.61	22.64	31.52	77.41	89.44	93.20
Improvements	-	-	-	<b>+4.19</b>	<b>+2.62</b>	<b>+2.07</b>	<b>+3.42</b>	<b>+1.42</b>	<b>+0.39</b>	<b>+12.61</b>	<b>+20.92</b>	<b>+28.65</b>	<b>+6.18</b>	<b>+3.67</b>	<b>+3.14</b>
Conv-AP [18]	2022	V	w/o	88.93	93.87	94.80	94.48	98.62	99.16	4.58	8.88	12.03	84.83	94.98	97.49
			w	<b>91.40</b>	<b>95.53</b>	<b>96.85</b>	<b>95.67</b>	<b>98.46</b>	99.03	<b>22.64</b>	<b>42.41</b>	<b>54.44</b>	89.85	<b>96.65</b>	<b>98.74</b>
Improvements	-	-	-	<b>+2.47</b>	<b>+1.65</b>	<b>+2.05</b>	<b>+1.19</b>	<b>-0.16</b>	<b>-0.13</b>	<b>+18.06</b>	<b>+33.53</b>	<b>+42.41</b>	<b>+5.02</b>	<b>+1.67</b>	<b>+1.25</b>
EigenPlaces [26]	2023	V	w/o	88.05	93.48	94.54	93.53	98.36	99.09	2.29	6.02	8.60	84.94	94.67	97.18
			w	90.85	94.36	95.93	95.37	98.11	99.09	14.61	25.21	35.82	<b>90.48</b>	96.23	98.12
Improvements	-	-	-	<b>+2.80</b>	<b>+0.88</b>	<b>+1.39</b>	<b>+1.84</b>	<b>-0.25</b>	<b>+0.00</b>	<b>+12.32</b>	<b>+19.19</b>	<b>+27.22</b>	<b>+5.54</b>	<b>+1.56</b>	<b>+0.94</b>
MixVPR [27]	2023	V	w/o	89.25	93.76	95.03	94.55	98.31	99.18	6.88	12.03	15.47	85.98	94.98	97.91
			w	90.85	94.39	95.72	95.46	98.44	<b>99.20</b>	16.91	25.21	31.52	89.12	94.35	97.49
Improvements	-	-	-	<b>+1.60</b>	<b>+0.63</b>	<b>+0.69</b>	<b>+0.91</b>	<b>+0.13</b>	<b>+0.02</b>	<b>+10.03</b>	<b>+13.18</b>	<b>+16.05</b>	<b>+3.14</b>	<b>-0.63</b>	<b>-0.42</b>

TABLE IV  
ABLATION OF SHARED BOTTOM BACKBONE.

#	Arch	BEV	shared backbone?	R@1	R@5	R@10	R <sup>E</sup> @1	R <sup>E</sup> @5	R <sup>E</sup> @10	R <sup>H</sup> @1	R <sup>H</sup> @5	R <sup>H</sup> @10	R <sup>SH</sup> @1	R <sup>SH</sup> @5	R <sup>SH</sup> @10
1	Single-input (baseline)	w/o	unshared	88.93	93.87	94.80	94.48	98.62	99.16	4.58	8.88	12.03	84.83	94.98	97.49
2	Single-input	w/o	shared	88.75	93.73	94.90	93.70	97.79	98.50	10.89	19.48	26.93	86.51	95.61	97.28
	Improvements	-	-	<b>-0.18</b>	<b>-0.15</b>	<b>+0.10</b>	<b>-0.78</b>	<b>-0.84</b>	<b>-0.66</b>	<b>+6.30</b>	<b>+10.60</b>	<b>+14.90</b>	<b>+1.67</b>	<b>+0.63</b>	<b>-0.21</b>
3	Dual-input	w	unshared	90.59	94.03	95.45	95.24	98.21	99.14	15.19	22.64	29.23	89.12	94.04	96.55
	Improvements	-	-	<b>+1.66</b>	<b>+0.16</b>	<b>+0.65</b>	<b>+0.76</b>	<b>-0.41</b>	<b>-0.02</b>	<b>+10.61</b>	<b>+13.76</b>	<b>+17.20</b>	<b>+4.29</b>	<b>-0.94</b>	<b>-0.94</b>
4	Single-input	w	shared	91.40	95.53	96.85	95.67	98.46	99.03	22.64	42.41	54.44	89.85	96.65	98.74
	Improvements	-	-	<b>+2.47</b>	<b>+1.65</b>	<b>+2.05</b>	<b>+1.19</b>	<b>-0.17</b>	<b>-0.13</b>	<b>+18.05</b>	<b>+33.52</b>	<b>+42.41</b>	<b>+5.02</b>	<b>+1.67</b>	<b>+1.26</b>

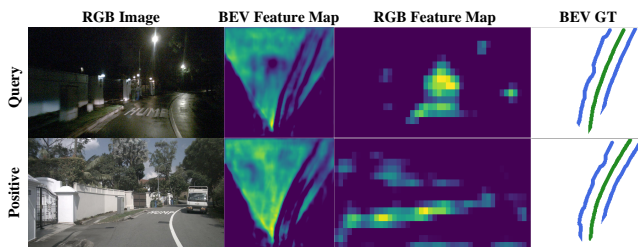


Fig. 4. Visualization comparisons of RGB and BEV features. Obviously, BEV features exhibit more structural characteristics than RGB features.

during the day and night, respectively. It is evident that under such conditions, the effectiveness of structural information in the BEV frame is far greater than that of appearance information in the RGB frame.

**Image Clarity Change.** The methods with added structural cues can also yield considerable performance enhancements in scenes where there is a substantial change in image clarity, with an average improvement of 5.62% on R<sup>SH</sup>@1 across different models. As shown in the third row of Fig. 3, compared with positive images, the query image is more blurry, but the overall image content remains basically unchanged. The semantic and texture information in certain areas is relatively complete and the structural information can

further assist in generating more comprehensive features.

These results demonstrate the importance of BEV representation in compensating for deficiencies in VPR.

#### D. Ablation Study

We perform all ablation experiments with Conv-AP as the baseline model.

**Shared Bottom Backbone.** To demonstrate the effectiveness of the shared bottom backbone, we intentionally degenerate our framework into two versions, as depicted in Table IV, one (#2) is single-input with a bottom backbone pre-trained through BEV generation but without structural stream, the other (#3) is dual-input with a bottom backbone not pre-trained via BEV generation. The results reveal that the shared bottom backbone helps visual stream learn fine-grained local features (#1 *v.s.* #2), especially map information such as lane divider, pedestrian crossing, and lane boundary in our work. This is more effective for hard scenes, but to some extent, it affects the effectiveness of global features in simple scenes. For #3, the dual-input network involves a visual stream and a structural stream, which, beyond appearance information, can provide more detailed BEV structural information, thereby resulting in greater

TABLE V  
ABLATION OF BEV TYPE.

#	Div.	P.C.	Bound.	R@1	R@5	R@10	R <sup>E</sup> @1	R <sup>E</sup> @5	R <sup>E</sup> @10	R <sup>H</sup> @1	R <sup>H</sup> @5	R <sup>H</sup> @10	R <sup>SH</sup> @1	R <sup>SH</sup> @5	R <sup>SH</sup> @10
1	-	-	-	88.93	93.87	94.80	94.48	98.62	99.16	4.58	8.88	12.03	84.83	94.98	97.49
2	✓	-	-	91.25	94.90	96.05	<b>96.09</b>	98.83	99.41	14.33	25.50	32.95	89.12	95.71	98.12
3	-	✓	-	89.96	94.21	95.56	95.19	98.36	99.08	9.46	22.35	30.66	86.72	94.56	97.28
4	-	-	✓	90.11	94.90	96.20	94.94	<b>98.84</b>	99.46	15.76	24.93	34.96	87.13	95.82	98.22
5	✓	✓	-	91.02	95.05	96.30	<b>96.09</b>	98.59	99.30	14.33	30.09	39.54	87.34	96.65	98.33
6	✓	-	✓	91.11	94.65	95.82	95.92	98.59	99.20	17.48	26.07	33.24	87.97	95.08	97.59
7	-	✓	✓	90.77	94.69	95.68	95.79	<b>98.84</b>	<b>99.48</b>	9.74	17.19	23.21	89.02	<b>97.07</b>	98.43
8	✓	✓	✓	<b>91.40</b>	<b>95.53</b>	<b>96.85</b>	95.67	98.46	99.03	<b>22.64</b>	<b>42.41</b>	<b>54.44</b>	<b>89.85</b>	96.65	<b>98.74</b>

performance improvements in hard and semi-hard scenes. Based on the above discussion, a shared bottom backbone and a structural stream can maximize the robustness of global features under different environments.

**BEV Types.** We then perform ablation experiments to study the impact of varying types of BEV supervised models on VPR. Given the restricted variety of map elements within the nuScenes dataset, we focus on three key static elements: lane divider, pedestrian crossing, and lane boundary. As depicted in Table V, when training without structural information, the baseline achieves 88.93% R@1 and 4.58% R<sup>H</sup>@1, respectively. When providing structural information of lane divider to the model, our method achieves gains of 2.32% and 9.75% on R@1 and R<sup>H</sup>@1. More types of BEV consistently improves our method, particularly benefiting the categories of lane divider and lane boundary, which can be attributed to the higher proportion of road divider and road boundary in the image compared to pedestrian crossing. While three types of static elements with structural characteristics can achieve the best performance improvement.

## V. CONCLUSIONS

In this paper, we propose a new BEV-enhanced VPR framework by exploiting the structural cues in BEV from a single monocular camera and introduce a new dataset for place recognition. The cores of our success lie in the introduction of BEV structural information and the promotion of the shared bottom backbone for local feature learning in the visual stream. Analytical experiments exhibit the superiority of BEV structural information in retrieving hard samples. We hope our work can enlighten more research on camera-based visual place recognition.

## REFERENCES

- [1] S. Lowry, N. Sünderhauf, P. Newman, J. J. Leonard, D. Cox, P. Corke, and M. J. Milford, "Visual place recognition: A survey," *IEEE transactions on robotics*, vol. 32, no. 1, pp. 1–19, 2015.
- [2] C. Masone and B. Caputo, "A survey on deep visual place recognition," *IEEE Access*, vol. 9, pp. 19 516–19 547, 2021.
- [3] X. Zhang, L. Wang, and Y. Su, "Visual place recognition: A survey from deep learning perspective," *Pattern Recognition*, vol. 113, p. 107760, 2021.
- [4] L. Luo, S. Zheng, Y. Li, Y. Fan, B. Yu, S.-Y. Cao, J. Li, and H.-L. Shen, "Bevplace: Learning lidar-based place recognition using bird's eye view images," in *Proceedings of the IEEE/CVF International Conference on Computer Vision*, 2023, pp. 8700–8709.
- [5] J. Komorowski, M. Wysoczańska, and T. Trzcinski, "Minkloc++: lidar and monocular image fusion for place recognition," in *2021 International Joint Conference on Neural Networks (IJCNN)*. IEEE, 2021, pp. 1–8.
- [6] H. Lai, P. Yin, and S. Scherer, "Adafusion: Visual-lidar fusion with adaptive weights for place recognition," *IEEE Robotics and Automation Letters*, vol. 7, no. 4, pp. 12 038–12 045, 2022.
- [7] Z. Zhou, J. Xu, G. Xiong, and J. Ma, "Lcpr: A multi-scale attention-based lidar-camera fusion network for place recognition," *IEEE Robotics and Automation Letters*, 2023.
- [8] H. Hu, Z. Qiao, M. Cheng, Z. Liu, and H. Wang, "Dasgil: Domain adaptation for semantic and geometric-aware image-based localization," *IEEE Transactions on Image Processing*, vol. 30, pp. 1342–1353, 2020.
- [9] A. Oertel, T. Cieslewski, and D. Scaramuzza, "Augmenting visual place recognition with structural cues," *IEEE Robotics and Automation Letters*, vol. 5, no. 4, pp. 5534–5541, 2020.
- [10] Y. Shen, S. Zhou, J. Fu, R. Wang, S. Chen, and N. Zheng, "Structvpr: Distill structural knowledge with weighting samples for visual place recognition," in *Proceedings of the IEEE/CVF Conference on Computer Vision and Pattern Recognition*, 2023, pp. 11 217–11 226.
- [11] A. Kirillov, E. Mintun, N. Ravi, H. Mao, C. Rolland, L. Gustafson, T. Xiao, S. Whitehead, A. C. Berg, W.-Y. Lo *et al.*, "Segment anything," *arXiv preprint arXiv:2304.02643*, 2023.
- [12] R. Arandjelovic, P. Gronat, A. Torii, T. Pajdla, and J. Sivic, "Netvlad: Cnn architecture for weakly supervised place recognition," in *Proceedings of the IEEE conference on computer vision and pattern recognition*, 2016, pp. 5297–5307.
- [13] J. Yu, C. Zhu, J. Zhang, Q. Huang, and D. Tao, "Spatial pyramid-enhanced netvlad with weighted triplet loss for place recognition," *IEEE transactions on neural networks and learning systems*, vol. 31, no. 2, pp. 661–674, 2019.
- [14] J. Zhang, Y. Cao, and Q. Wu, "Vector of locally and adaptively aggregated descriptors for image feature representation," *Pattern Recognition*, vol. 116, p. 107952, 2021.
- [15] F. Radenović, G. Toliás, and O. Chum, "Fine-tuning cnn image retrieval with no human annotation," *IEEE transactions on pattern analysis and machine intelligence*, vol. 41, no. 7, pp. 1655–1668, 2018.
- [16] G. Berton, C. Masone, and B. Caputo, "Rethinking visual geo-localization for large-scale applications," in *Proceedings of the IEEE/CVF Conference on Computer Vision and Pattern Recognition*, 2022, pp. 4878–4888.
- [17] R. Wang, Y. Shen, W. Zuo, S. Zhou, and N. Zheng, "Transvpr: Transformer-based place recognition with multi-level attention aggregation," in *Proceedings of the IEEE/CVF Conference on Computer Vision and Pattern Recognition*, 2022, pp. 13 648–13 657.
- [18] A. Ali-bey, B. Chaib-draa, and P. Giguère, "Gsv-cities: Toward appropriate supervised visual place recognition," *Neurocomputing*, vol. 513, pp. 194–203, 2022.
- [19] Y. Lu, F. Yang, F. Chen, and D. Xie, "Pic-net: Point cloud and image collaboration network for large-scale place recognition," *arXiv preprint arXiv:2008.00658*, 2020.
- [20] S. Ratz, M. Dymczyk, R. Siegwart, and R. Dubé, "Oneshot global localization: Instant lidar-visual pose estimation," in *2020 IEEE International conference on Robotics and Automation (ICRA)*. IEEE, 2020, pp. 5415–5421.
- [21] Y. Pan, X. Xu, W. Li, Y. Cui, Y. Wang, and R. Xiong, "Coral: Colored structural representation for bi-modal place recognition," in



- 2021 *IEEE/RSJ International Conference on Intelligent Robots and Systems (IROS)*. IEEE, 2021, pp. 2084–2091.
- [22] C. Qin, Y. Zhang, Y. Liu, D. Zhu, S. A. Coleman, and D. Kerr, “Structure-aware feature disentanglement with knowledge transfer for appearance-changing place recognition,” *IEEE Transactions on Neural Networks and Learning Systems*, 2021.
- [23] J. Phillion and S. Fidler, “Lift, splat, shoot: Encoding images from arbitrary camera rigs by implicitly unprojecting to 3d,” in *Computer Vision—ECCV 2020: 16th European Conference, Glasgow, UK, August 23–28, 2020, Proceedings, Part XIV 16*. Springer, 2020, pp. 194–210.
- [24] Y.-H. Wu, Y. Liu, J. Xu, J.-W. Bian, Y.-C. Gu, and M.-M. Cheng, “Mobilesal: Extremely efficient rgb-d salient object detection,” *IEEE Transactions on Pattern Analysis and Machine Intelligence*, vol. 44, no. 12, pp. 10 261–10 269, 2021.
- [25] A. B. Yandex and V. Lempitsky, “Aggregating local deep features for image retrieval,” in *2015 IEEE International Conference on Computer Vision (ICCV)*, 2015, pp. 1269–1277.
- [26] G. Berton, G. Trivigno, B. Caputo, and C. Masone, “Eigenplaces: Training viewpoint robust models for visual place recognition,” in *Proceedings of the IEEE/CVF International Conference on Computer Vision*, 2023, pp. 11 080–11 090.
- [27] A. Ali-Bey, B. Chaib-Draa, and P. Giguere, “Mixvpr: Feature mixing for visual place recognition,” in *Proceedings of the IEEE/CVF Winter Conference on Applications of Computer Vision*, 2023, pp. 2998–3007.
- [28] Q. Li, Y. Wang, Y. Wang, and H. Zhao, “Hdmapnet: An online hd map construction and evaluation framework,” in *2022 International Conference on Robotics and Automation (ICRA)*. IEEE, 2022, pp. 4628–4634.
- [29] H. Caesar, V. Bankiti, A. H. Lang, S. Vora, V. E. Liong, Q. Xu, A. Krishnan, Y. Pan, G. Baldan, and O. Beijbom, “nusenes: A multimodal dataset for autonomous driving,” in *Proceedings of the IEEE/CVF conference on computer vision and pattern recognition*, 2020, pp. 11 621–11 631.